

Enhanced Hydrogen Gas Detection Using SAW Sensor Through Oxygen Pre-Treatment

Armando Ayes
Frontier Institute for Research in
Sensor Technologies
Dept. of Electrical & Comp. Eng.
University of Maine
Orono ME, USA
armando.ayes@maine.edu

Paul R. Ohodnicki
National Energy Technology
Laboratory
U.S. Dept. of Energy
Pittsburgh PA, USA
Paul.Ohodnicki@netl.doe.gov

Robert J. Lad
Frontier Institute for Research in
Sensor Technologies
Dept. of Physics & Astronomy
University of Maine
Orono ME, USA
rjlad@maine.edu

Mauricio Pereira da Cunha
Frontier Institute for Research in
Sensor Technologies
Dept. of Electrical & Comp. Eng.
University of Maine
Orono ME, USA
mdacunha@maine.edu

Abstract—Hydrogen gas sensing is crucial in a variety of applications, including power generation, fuel cells, automotive, metallurgic and manufacturing industries. Some of the requirements for a hydrogen sensor are reliability, robustness, stability, fast response and recovery times. Surface acoustic wave (SAW) technology can offer these characteristics, and others such as small size and weight, wireless operation capability including multiple sensor interrogation, mass production reproducibility and low cost. In this work, an improvement in room temperature H₂ gas sensor response time and stability is reported through the use of O₂ treatments. The exposure to O₂, after interaction with H₂, reconditions the Pt-Al₂O₃ composite thin-film used both as the electrode and H₂ sensing layer. As a result, the SAW sensor frequency response recovery is over five times larger during the initial 20 minutes when compared to the exposure to N₂ inert gas. In addition, the O₂ treatment allows the recovery of the sensor to a state close to the one prior to the reduction by H₂ within about an hour, thus leading to a stable device response, which is very difficult to achieve under the inert N₂ environment even after tens of hours. The method is thus very promising in recovering the surface of sensing devices which rely on metallic composite electrodes and oxide films exposed to reducing environment.

Keywords—Pt-Al₂O₃ composite electrodes; Hydrogen sensor; SAW gas sensor; Oxygen treatments; Sensor recovery time

I. INTRODUCTION

There is a continued need to improve the performance of hydrogen sensors regarding safety monitoring (concentrations <10%) and full range detection functionality (1-100%) for a variety of applications such as fuel cell, coal mining, power plants, aerospace, and nuclear reactor safety [1]. Important sensor parameters, especially regarding sensors to be used for hydrogen safety, are sensor response time, recovery time, stability, robustness, extended life-time, and reliability in a variety of environments [2]. Surface Acoustic Wave (SAW) sensor technology can satisfy these needs, and in addition offers other capabilities, such as the possibility of wireless and passive operation (no batteries required), wafer-scale fabrication, reduced size and weight, and relative simplicity in fabrication (metallic layer on top of piezoelectric crystal) [1,3]. Hydrogen SAW resonators (SAWRs) sensors using Pt electrodes on langasite (LGS) piezoelectric crystal has been reported in [4].

This work has been funded by the U.S. Department of Energy/National Energy Technology Laboratory (NETL) under grant number DE-FE0026217

Oxygen surface treatments for sensor conditioning have been explored using Pd and AuPd nanoparticles in silica based optical fiber sensors [5].

In this work, oxygen gas has been used at room temperature to enhance the recovery time of SAWR H₂ sensors that employ a Pt-Al₂O₃ composite thin film structure as both electrode and H₂ sensing layer. After exposure to O₂ for 20min, the SAWR frequency response recovery is over five times larger than employing N₂. In addition, the exposure to O₂ allows the sensor to reach a recovery state sooner (after a few hours at room temperature) by replenishing the oxygen deficiency within the Pt-Al₂O₃ composite film resulting from the H₂ reduction, as opposed to at least tens of hours in inert N₂ gas. As a result of reducing the sensor recovery time and increasing the frequency variation response to repeated H₂ exposure, the exposure to O₂ also increases the sensor sensitivity and dynamic range. The H₂ sensor phenomenon and procedure reported in this work using Pt-Al₂O₃ composite electrodes on the SAW platform can be extended to other types of sensors, such as resistive sensors, which employ composite films [6] or oxides as sensing layers in reducing environments.

II. SAWR FABRICATION

The one-port SAWRs utilized in this work were fabricated on the commercially available LGS wafers oriented along Euler angles {0°, 138.5°, 26.7°}. The devices were manufactured in the University of Maine cleanroom fabrication facilities using a lift-off photolithographic process and the deposition of Pt-Al₂O₃ composite film consisting of 82 at% Pt and 18 at% Al₂O₃, fabricated by e-beam co-evaporation of Pt and Al in oxygen environment (10⁻⁵ Torr partial pressure) [6]-[9]. The Pt-Al₂O₃ film, similar to Pt-Al₂O₃ films reported in [8, 9], was used as electrodes, reflectors and as the H₂ sensing element. The SAWRs were fabricated with a 1:1 mark-to-space ratio, interdigitated transducers (IDT) periodicity 2p of 14μm (nominal operating frequency around 190MHz), acoustic aperture W of 51 wavelengths (λ), 161 IDT electrodes, and 411 open-circuited electrodes used as reflectors on each side. After fabrication, each wafer of SAWR devices was cleaned with acetone, iso-propanol, methanol and de-ionized (DI) water, and dried with N₂. All of the devices were heated in an alumina crucible to 800°C for four hours for annealing and electrical activation of the Pt-Al₂O₃ composite film. The wafers were then

covered in photoresist and diced to an individual SAWR device dimension of approximately $10 \times 3 \times 0.5 \text{ mm}^3$.

III. EXPERIMENTAL SETUP

Fig. 1 shows the stainless-steel box with two gas chambers (57mm x 24mm x 12.5mm each) utilized for the gas-cycling tests reported in this work. Two SAWRs and one K-type thermocouple (TC) were mounted in each chamber. The TC junction was placed on top of a piece of LGS to measure temperatures comparable to the ones seen by the SAW devices. The SAWRs were held in place by 4mil Pt wires welded to the box using a Unitek resistance welder. Electrical connections between the SAWRs and the Inconel coaxial cables shown in Fig. 1 were performed using the same welder and 1mil Pt wires.

Fig. 2 shows the schematic of the experimental setup, and Fig. 3 shows images of the gas delivery system and measurement equipment utilized. Two Tylan mass-flow controllers (one for each chamber) with a mass flow capacity of 1 standard liter per minute and three AP Tech (Advanced Pressure Technology) valves were used to deliver N_2 gas (>99.999% purity) (henceforth referred to as N_2), 4.7 grade O_2 (henceforth O_2) and a 4%/96% H_2/N_2 mixture (henceforth H_2). All gases were delivered with a flow rate of 950scm. The SAWRs were interrogated by an E5071C Vector Network Analyzer (VNA) with the aid of a Mini-Circuits 4-way RF switch (RF MUX). Frequency sweeps of 6MHz centered at 191MHz with 10001 points and an Intermediate Frequency (IF) bandwidth of 1kHz were used for the tests reported. Parabolic fitting over a bandwidth of 25kHz around the resonant frequency was used for the extraction of the SAWR resonant frequency. The temperature was recorded before and after each device was interrogated and both temperature values averaged to represent the temperature of each measurement. The room temperature averaged 22.1°C during the entire test, with a maximum temperature variation of about 2.1°C during a 20 min period and a minimum and maximum room temperature of 18°C and 26°C for the entire test, as shown in Fig. 4 right vertical axis. The SAWRs fabricated on LGS orientation mentioned in Section II are close to being temperature-compensated around room temperature, with a measured temperature sensitivity of $-0.7 \text{ kHz}/^\circ\text{C}$ [10], which translates the maximum 2.1°C variation during 20min to $\sim 1.5 \text{ kHz}$. After a change in gas species, the SAWRs were interrogated every minute for 5 minutes, after which there was one interrogation every 5 minutes until the next change in gas species.

IV. RESULTS AND DISCUSSION

Fig. 4 depicts the SAWR resonant frequency (left vertical axis) measured at room temperature as a function of time under the exposure to N_2 , O_2 , and H_2 , cycled as shown in the right vertical axis. From Fig. 4, one can see that the exposure to oxygen (periods Ox_1 , Ox_2 , and Ox_3) had a significant impact on the SAWR frequency recovery after periods of exposure to H_2 (Periods denoted as R in Fig. 4).

As indicated in Fig. 4, the initialization sequence consisted of 30 min in N_2 flow, followed by two 20min cycles between N_2 and O_2 , and ended with $4\frac{1}{2}$ hours in N_2 . A reduction sequence R followed, which consisted of three 20-min H_2 and N_2 cycles and finalized by a 1-hour N_2 purging period. The longer N_2 purging

period was aimed at mitigating the formation of water if O_2 were to be introduced just after the H_2 cycle. The initial H_2 exposure caused a frequency shift of approximately 30kHz, whereas the subsequent removal of H_2 with 20min N_2 periods caused approximately 4kHz frequency recovery shifts. This recovery during the N_2 periods could be due to a series of factors, including limited purity of the N_2 used or minor leaks in the gas

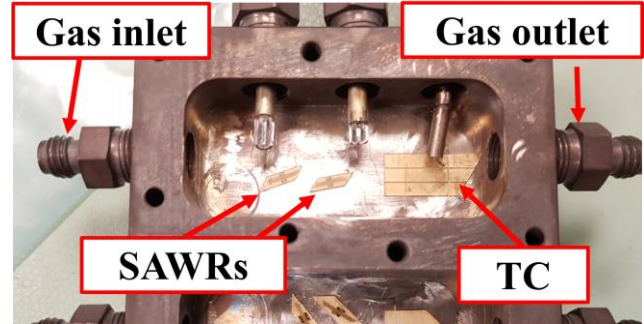


Fig. 1. SAWRs and TC mounted in stainless steel gas testing chamber.

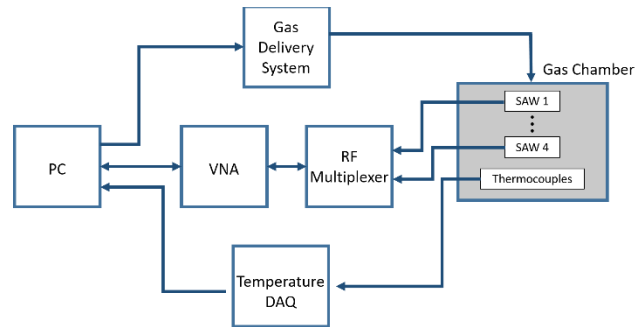


Fig. 2. Schematic of the experimental setup.

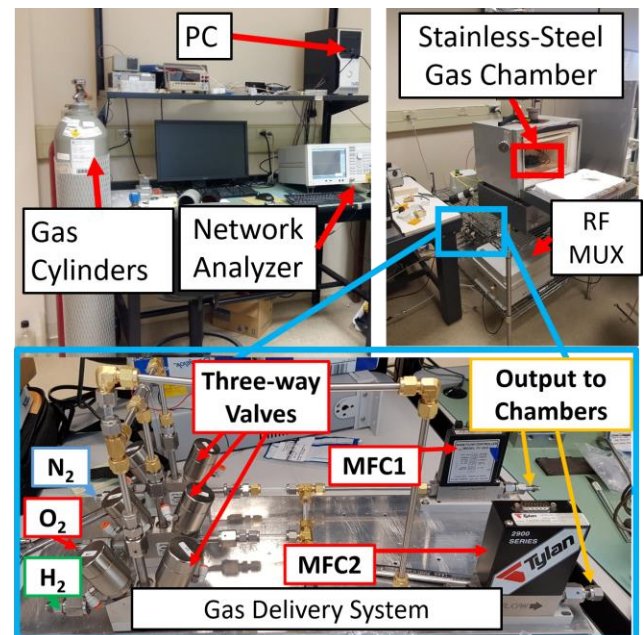


Fig. 3. Images of gas delivery system and experimental setup

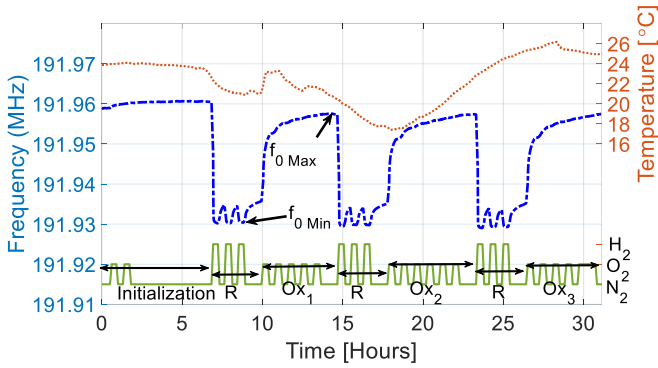


Fig. 4. Left axis: SAWR resonant frequency response (blue dotted-dashed line) vs. time under reduction and oxidation cycles at room temperature; $f_{0\text{Max}}=191.958\text{MHz}$, $f_{0\text{Min}} = 191.930\text{MHz}$. Right axis top: temperature variation during the test (red dotted line). Right axis bottom: H_2 , O_2 , and N_2 gas species cycling (solid green line).

system or outgassing which could allow O_2 or humidity into the chamber. Following the reduction, the oxidation sequence Ox_1 takes place, which consists of five O_2 and N_2 cycles finalized by a 1-hour N_2 purging period. In total, the 1-hour N_2 period and the Ox_1 sequence caused a recovery of approximately 27kHz. The next reduction sequences repeated the first one, with the following differences: the second oxidation sequence Ox_2 counted with a sixth N_2/O_2 cycle, and the third one (labeled Ox_3 in the figure) had four N_2/O_2 cycles and a final one-hour exposure to O_2 . The different oxidations sequences in Ox_2 and Ox_3 were performed to verify that the sensor recovery was not affected by additional exposure to O_2 . As shown in from Fig. 4, the extra O_2 cycling period in Ox_2 and the longer last O_2 period in Ox_3 did not significantly change the value of the maximum resonant frequency $f_{0\text{Max}}$.

Fig. 5 zooms in on a particular section of Fig. 4, that is, the end of the first reduction cycle R and the oxidation period Ox_1 . The intent was to quantify the improvement in the SAWR frequency response recovery time after exposure to H_2 , when compared to using N_2 purging alone. The vertical axis in Fig. 5 plots the normalized resonant frequency, f_n , defined as

$$f_n = 100 \frac{f - f_{0\text{Min}}}{f_{0\text{Max}} - f_{0\text{Min}}} [\%], \quad (1)$$

where, as defined in Fig. 4, $f_{0\text{Min}}$ is minimum frequency at the end of the last exposure to H_2 in the first reduction cycle and right before the 1-hour N_2 purging period, whereas $f_{0\text{Max}}$ is the maximum frequency after Ox_1 . Feature A in Fig. 5 is the 1-hour N_2 purging period at the end of the first reduction cycle, and Feature B is the 1-hour period consisting of a 20-min exposure to O_2 , followed by 20-min in N_2 and another 20-min in O_2 . Exponential fittings were used on the first data points of both Feature A and Feature B, as indicated in Figs. 4 and 5, in order to extend the curves to the value of $f_{0\text{Min}}$. One can note that there are lag times between the switching to N_2 in Period A and to O_2 in Period B and the fitted value of zero f_n . These lag times are due to the purging of the previous gas in the chamber, that is, either H_2 or N_2 , respectively.

Fig. 6 plots the normalized measured frequency f_n for Features A and B and the respective fitted responses on the same time scale. As can be observed in Fig. 6, after the first O_2 cycle at the 20-min mark, the sensor recovered to 78% of $f_{0\text{Max}}$, as opposed to 15% for N_2 alone, for a five-times larger frequency recovery for the referred 20-minute period. After 68 min in the O_2/N_2 cycling, the sensor recovered 90% of $f_{0\text{Max}}$, while in N_2 that number drops to 21%.

In N_2 , the SAWR frequency response went from an exponential behavior during the first 6 minutes to a square root behavior with time [11] ($0.99 R^2$ correlation), as shown by the fitting in Fig. 6. Assuming that this time dependence continues in the long run, it would take over 51h for SAWR frequency response to reach 90% of $f_{0\text{Max}}$, which would be 45 times longer than the respective time recovery to 90% of $f_{0\text{Max}}$ achieved through the O_2/N_2 cycling, and even longer to recover to full $f_{0\text{Max}}$.

V. CONCLUSION

This work highlights the relevance of conditioning the surface of the $\text{Pt-Al}_2\text{O}_3$ composite thin-film electrodes used on SAWR sensors to detect H_2 by employing O_2 treatments at room temperature. The O_2 technique showed that a five-fold larger SAWR frequency recover was achieved during a period of

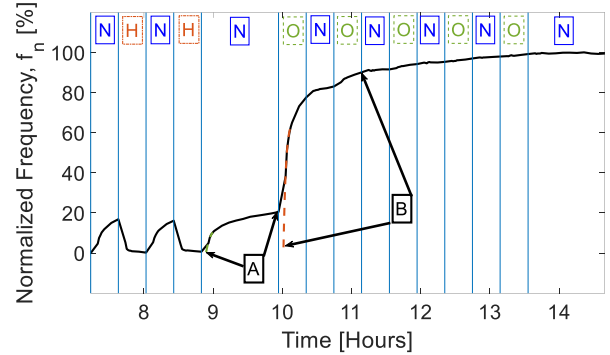


Fig. 5. Normalized SAWR frequency response according to Eq. 1 at the end of the first reduction cycle R and the oxidation period Ox_1 . Feature A is the sensor recovery after one hour purging in N_2 , Feature B is sensor recovery after one-hour period in O_2/N_2 cycling indicated. Exponential fitting was used to approximate a start time for the recovery as discussed in the text.

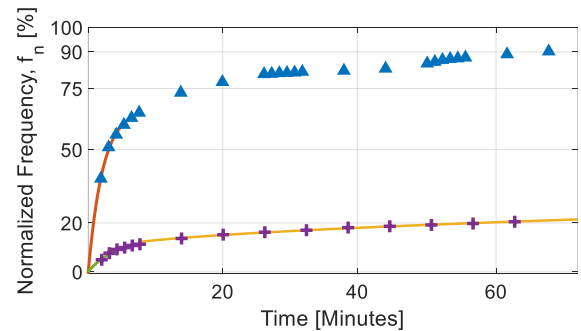


Fig. 6. Comparison of SAWR normalized frequency recovery under exposure to the O_2/N_2 cycles (blue triangles) and under N_2 only (purple crosses) for about one hour periods. Discrete points are measured data; solid curves are exponential fitting for both curves approaching zero min and $t^{1/2}$ fitting for the N_2 curve after six minutes.

20 min when compared to the exposure to inert N₂ gas alone. After 68 minutes, 90% of the sensor frequency range was recovered as opposed to only 21% in N₂. Moreover, the oxidizing treatments allowed stable response of the sensor after a few hours, by replenishing the oxygen deficiency in the Pt-Al₂O₃ composite film caused by the H₂ reduction, which is not possible with the inert N₂ gas, thus diminishing the surface recovery time by tens of hours and allowing repeated sensor use in shorter periods with higher sensitivity and dynamic range.

It may be possible to extend the improved H₂ sensing behavior and recovery time caused by O₂ conditioning of the Pt-Al₂O₃ composite electrodes to other types of oxide-based sensing layers and sensor devices to improve their performance in reducing environments.

DISCLAIMER

This work was supported by U.S. Department of Energy Award #: DE-FE0026217. Disclaimer: This report was prepared as an account of work sponsored by an agency of the United States Government. Neither the United States Government nor any agency thereof, nor any of their employees, makes any warranty, express or implied, or assumes any legal liability or responsibility for the accuracy, completeness, or usefulness of any information, apparatus, product, or process disclosed, or represents that its use would not infringe privately owned rights. Reference herein to any specific commercial product, process, or service by trade name, trademark, manufacturer, or otherwise does not necessarily constitute or imply its endorsement, recommendation, or favoring by the United States Government or any agency thereof. The views and opinions of authors expressed herein do not necessarily state or reflect those of the United States Government or any agency thereof.

REFERENCES

- [1] T. Hübert, L. Boon-Brett, G. Black, and U. Banach, "Hydrogen sensors - A review," *Sensors Actuators, B Chem.*, vol. 157, no. 2, pp. 329–352, Oct. 2011.
- [2] W. J. Buttner, M. B. Post, R. Burgess, and C. Rivkin, "An overview of hydrogen safety sensors and requirements," *Int. J. Hydrogen Energy*, vol. 36, no. 3, pp. 2462–2470, 2011.
- [3] L. Bo *et al.*, "Surface acoustic wave devices for sensor applications," *J. Semicond.*, vol. 37, no. 2, pp. 2–9, 2016.
- [4] J. A. Thiele and M. Pereira da Cunha, "High temperature LGS SAW gas sensor," *Sensors Actuators, B Chem.*, vol. 113, no. 2, pp. 816–822, Feb. 2006.
- [5] P. R. Ohodnicki, J. P. Baltrus, and T. D. Brown, "Pd/SiO₂ and AuPd/SiO₂ nanocomposite-based optical fiber sensors for H₂ sensing applications," *Sensors Actuators, B Chem.*, vol. 214, pp. 159–168, 2015.
- [6] D. J. Frankel, S. C. Moulzolf, M. Pereira da Cunha, and R. J. Lad, "Influence of composition and multilayer architecture on electrical conductivity of high temperature Pt-alloy films," *Surf. Coatings Technol.*, vol. 284, pp. 215–221, 2015.
- [7] M. Pereira da Cunha, "Wireless sensing in hostile environments," *IEEE Int. Ultrason. Symp. IUS*, 2013, pp. 1337–1346.
- [8] A. Ayes, A. Maskay and M. Pereira da Cunha, "Predicted and measured temperature compensated surface acoustic wave devices for high-temperature applications" *Electronics Letters* vol. 53 no. 11, pp. 699-700, 2017.
- [9] A. Maskay, A. Ayes, and M. Pereira Da Cunha, "Stability of Pt/Al₂O₃-based electrode langasite SAW sensors with Al₂O₃ capping layer and yttria-stabilized zirconia sensing layer," *IEEE Int. Ultrason. Symp. IUS*, 2017, pp. 2–5.
- [10] A. Ayes and M. Pereira da Cunha, "Influence of Langasite Crystal Orientation on Hydrogen gas Detection up to 400°C," *IEEE Int. Ultrason. Symp. IUS*, 2019 (*in press: this conference*).
- [11] A. Reghu, L. J. Legore, J. F. Vetelino, R. J. Lad, and B. G. Frederick, "Distinguishing bulk conduction from band bending transduction mechanisms in chemiresistive metal oxide gas sensors," *J. Phys. Chem. C*, vol. 122, no. 19, pp. 10607–10620, 2018.